Numerical Simulation of Aerodynamic Characteristics of Helicopter Rotor with Tip Slots

Chen Rongqian[1*], *Wang Xu*[2], *Cheng Qiyou*[3], *Zhu Chengxiang*[1], *You Yancheng*[1]

1. School of Aerospace Engineering, Xiamen University, Xiamen 361005, P. R. China;
2. AECC Hunan Aviation Powerplant Research Institute, Zhuzhou 412002, P. R. China;
3. Science and Technology on Rotorcraft Aeromechanics Laboratory, China Helicopter Research and Development Institute, Jingdezhen 333001, P. R. China

(Received 14 August 2017; revised 22 May 2018; accepted 5 December 2018)

Abstract: Effects of tip slots on the aerodynamic characteristics of helicopter rotor were investigated numerically by solving three-dimensional Navier-Stokes equations based on unstructured overset grids algorithm. Improved delayed detached eddy simulation (IDDES) based on the Spalart-Allmaras turbulence model and adaptive grid refinement technique were employed. Several slots in the rotor blade tip were designed on the base of Caradonna-Tung rotor to study the effect of tip slots. Numerical results show that tip slots are able to introduce the airflow from the leading edge and turn it in the spanwise direction to be ejected out of the face at the rotor blade tip, which can reduce the strength of the rotor blade tip vortex and accelerate the dissipation process. Although tip slots may lead to the decrease of airfoils' lift coefficient at the root of the rotor blade, it can increase the lift coefficient of airfoils at the rotor blade tip, so the lift of the rotor with tip slots is almost the same as that of the rotor without tip slots. In addition, tip slots can also reduce the intensity of the tip shock wave, which is beneficial to reduce the wave drag of the rotor.

Key words: tip slots; tip-vortex alleviation; helicopter rotor; numerical simulation

CLC number: V211.5 **Document code**: A **Article ID**: 1005-1120(2018)06-0942-10

0 Introduction

Compared with fixed wing aircrafts, due to the unique advantages of vertical takeoffs and landing, good maneuverability and hovering flight, helicopters are widely used on civil and military fields. Blade-vortex interaction (BVI) appears when helicopter rotating blade encounters the trailing wake generated from the front rotor blade[1], which makes helicopter rotor blade vibrate violently and generate strong noise. BVI is a serious problem for helicopter rotor structure and is always the difficulty in the research of rotor aerodynamics and aeroacoustics due to its complexity.

With regard to the BVI alleviation, many measures have been proposed, including optimizing the tip shape, installing the tip vortex alleviation equipment and so on. Although optimizing the tip shape, such as swept, tapered or anhedral blade tips[2,3], has some effects on BVI alleviation, these types of rotor blade tips are not able to balance the goals of improving the aerodynamic performance and reducing the vibration. Installing the tip vortex alleviation equipment, such as trailing edge spoiler, blade tip winglet or endplate[4], cannot work well, too. Trailing edge spoiler can reduce the strength of the blade tip vortex, while the profile drag of the rotor blade is very large, which causes aerodynamic performance of helicopter rotor to descend. Blade tip winglet can divide the original single tip vortex into

* Corresponding author, E-mail address: rqchen@xmu.edu.cn.

How to cite this article: Chen Rongqian, Wang Xu, Cheng Qiyou, et al. Numerical simulation of aerodynamic characteristics of helicopter rotor with tip slots[J]. Trans. Nanjing Univ. Aero. Astro., 2018,35(6):942-951.
http://dx.doi.org/10.16356/j.1005-1120.2018.06.942

two vortices and make use of the viscous effect to accelerate the dissipation of the blade tip vortex. However, practical application shows that the effect of the method on BVI alleviation is not obvious. With the development of new material and control technology, many new methods have been proposed, such as higher-harmonic pitch control (HHC), individual blade control (IBC), and active flap control (ACF)[5-7]. Nonetheless, it is difficult for these methods to be applied to engineering problems. In recent years, an effective method of the BVI alleviation based on blade tip slots has been proposed by Han[8-11]. Several slots in the rotor blade tip are designed. The air flows into the slot entrance at the leading edge of the blade and out of the slot exit at the side of the blade tip, forming a momentum jet, so as to alleviate the blade tip vortex. The method is easy to realize and with no need to add additional complex control system, so it is a potential method for BVI alleviation. Due to the limitations of experimental diagnostic tools, the mechanism of tip slots' effect on the aerodynamic characteristics of helicopter rotor has not been clarified, which is in urgent need of carrying out relevant research.

1 Numerical Methods

Three-dimensional Navier-Stokes equations based on unstructured overset grids algorithm were solved using the finite volume method. The inviscid fluxes were calculated using second-order central scheme with artificial dissipation, and dual-time stepping method was applied for the unsteady simulations. No-slip boundary condition was used for the wall boundary and non-reflecting boundary condition was used for the far-field boundary. Improved delayed detached eddy simulation (IDDES) based on Spalart-Allmaras turbulence model was used[12]. IDDES is a type of hybrid RANS/LES model, which distinguishes the RANS and LES computational domain automatically by partition scale $\tilde{d}$ to realize smooth transformation between RANS and LES in the boundary layer. The model is originated from detached eddy simulation (DES) model[13,14].

For the early DES[14] model, the definition of $\tilde{d}$ is

$$\tilde{d}=\min(d_{\mathrm{w}},C_{\mathrm{DES}}\Delta) \tag{1}$$

where d_{w} represents the distance to the wall, Δ is grid scale, and C_{DES} is a model parameter.

Delayed detached eddy simulation (DDES) model[15] changed the partition scale $\tilde{d}$ based on DES.

$$\tilde{d}=d_{\mathrm{w}}-f_d\max(0,d_{\mathrm{w}}-C_{\mathrm{DES}}\Delta) \tag{2}$$

For IDDES model, partition scale $\tilde{d}$ is defined as

$$\tilde{d}=\tilde{f}_d(1+f_e)d_{\mathrm{RANS}}+(1-\tilde{f}_d)d_{\mathrm{LES}} \tag{3}$$

where d_{RANS} represents RANS scale and d_{LES} represents LES scale.

$$\tilde{f}_d=\max\{(1-f_{dt}),f_B\} \tag{4}$$

$$f_B=\min\{2\exp(-9\alpha^2),1.0\} \tag{5}$$

$$\alpha=0.25-d_{\mathrm{w}}/h_{\max} \tag{6}$$

$$f_{dt}=1-\tanh[(8r_{dt})^3] \tag{7}$$

$$r_{dt}=\frac{\upsilon_t}{\kappa^2 d_{\mathrm{w}}^2\max\{[\sum_{i,j}(\partial u_i/\partial x_j)^2]^{1/2},10^{-10}\}} \tag{8}$$

where υ_t is eddy viscosity coefficient, $\partial u_i/\partial x_j$ is velocity gradient, and $\kappa=0.41$.

When incoming flow contains turbulent fluctuation, r_{dt} is much less than 1, f_{dt} is close to 1, and $\tilde{f}_d=f_B$, partition scale $\tilde{d}$ is defined as

$$\tilde{d}=d_{\mathrm{WMLES}}=f_B(1+f_e)d_{\mathrm{RANS}}+(1-f_B)d_{\mathrm{LES}} \tag{9}$$

When $f_e=0$, partition scale $\tilde{d}$ is defined as

$$\tilde{d}=d_{\mathrm{DDES}}=\tilde{f}_d d_{\mathrm{RANS}}+(1-\tilde{f}_d)d_{\mathrm{LES}} \tag{10}$$

Computational domain of the rotor was divided into rotating domain and static domain due to the use of the unstructured overset grids algorithm, and the grids were generated respectively in each sub-domain. The rotating domain contained the rotor and the static domain contained a hole, and there was an overlapping domain between the two domains. The information transmission between the two domains was carried out by the search and interpolation of the two sets of grids. Adaptive grid refinement technique was used during the unsteady computation to improve computational accuracy and better capture tip vortex. The grid was automatically refined where the gradient of the flow field parameter was large. The overset grids algorithm and the adaptive grid

refinement technique had been validated in the previous work[16].

2 Computational Model and Grids

In order to compare with the experimental data, Caradonna-Tung (C-T) rotor was used as the original configuration[17], as shown in Fig. 1 (a). The radius of the rotor is 1.143 m, and the aspect ratio is 6. On the basis of the C-T rotor, the slot system including three slots (circular pipes), which bypass a slight amount of the flow through the leading edge and turn it in the spanwise direction to be ejected out of the face at the blade tip, was designed, as shown in Fig. 1(b). The three slots are three concentric arcs. The diameter of the slot is $0.067C$, and the space between two adjacent slots is $0.157C$, where C is the chord length. The hovering condition was chosen for the simulation, which was at a blade tip Mach number of 0.877, a collective pitch angle of 8°, and the rotation speed is 2 500 RPM.

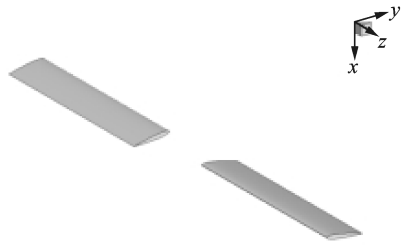

(a) Caradonna-Tung rotor

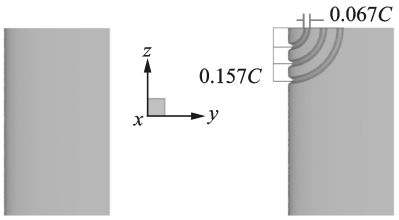

(b) Baseline tip and slotted tip

Fig. 1 Computational model

The computational grid was composed of two sets of grid: the rotor grid and the background grid, and there was an overlapping domain between the two domains, as shown in Fig. 2. The numbers of the rotor grid cells and background grid cells were about 5.4 million and 1.5 million, respectively. During the unsteady simulation, the grid was adapted according to the gradient of the flow field parameter.

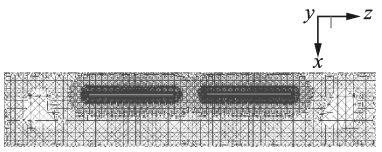

(a) Rotor grid

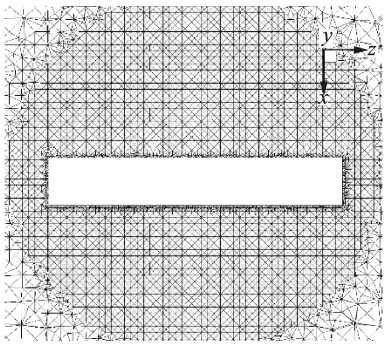

(b) Background grid

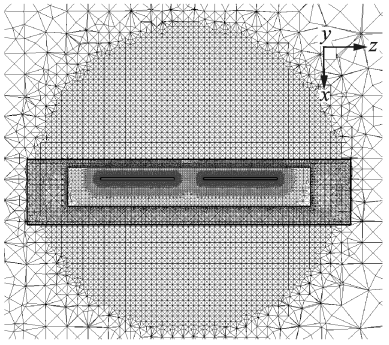

(c) Chimera grid

Fig. 2 Computational grids

3 Results and Discussion

3.1 Validation

In order to capture the vortex structure well, the adaptive grid refinement technique was used. Fig. 3(a) shows the adaptive refined grid and Fig. 3(b) shows the vorticity distribution of xz cross section, where the coordinate is nondimensionalized with the rotor radius R. It can be seen that the adaptive grid refinement technique provides good technical support for the simulation of high-resolution blade tip vortex.

Fig. 4 shows the Mach number distribution of the rotor without slots at xz section. Fig. 5 shows streamlines of the rotor without tip slots. As shown in the figures, when the air flows through the rotor, it is accelerated and the stream tube contracts according to the law of mass conservation.

Fig. 6 shows the distribution of surface pres-

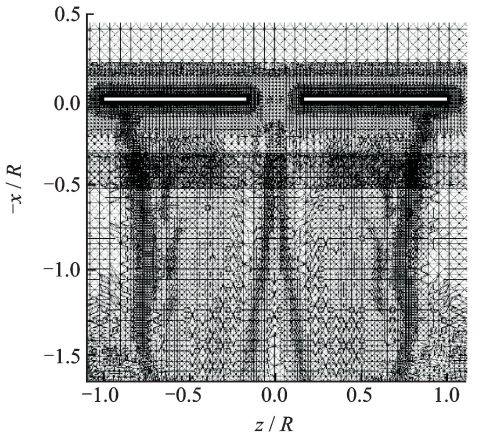

(a) Adaptive refined grid

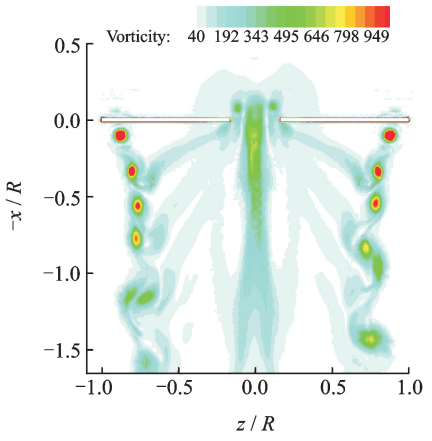

(b) Vorticity distribution of the xz cross section

Fig. 3 Adaptive refined grid and the vorticity distribution

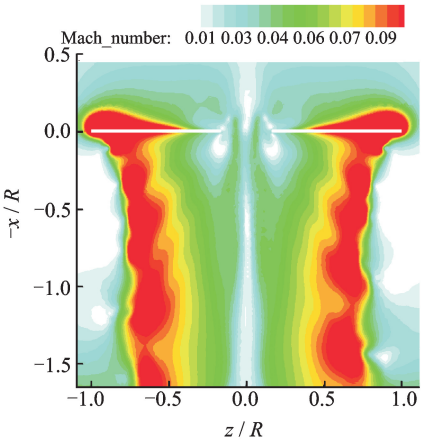

Fig. 4 Mach number distribution of the xz cross section

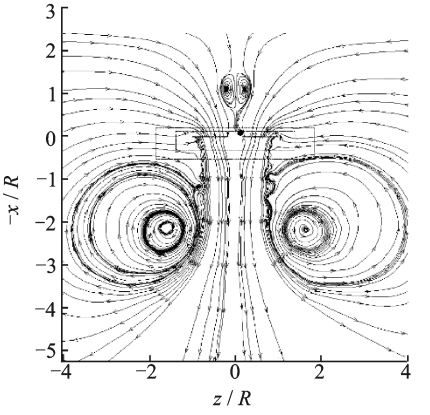

Fig. 5 Streamline distribution of the xz cross section

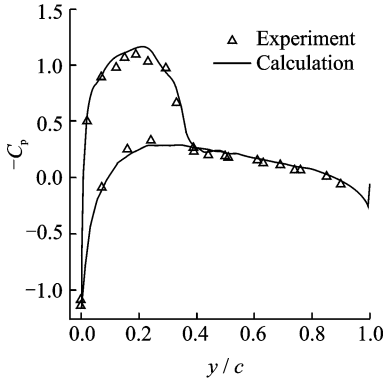

(a) 0.96R

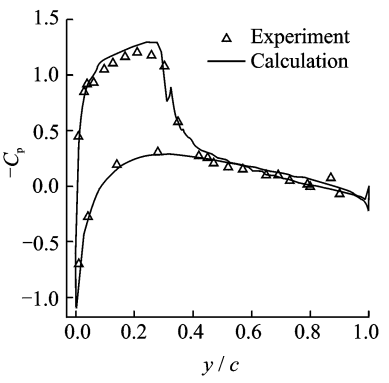

(b) 0.89R

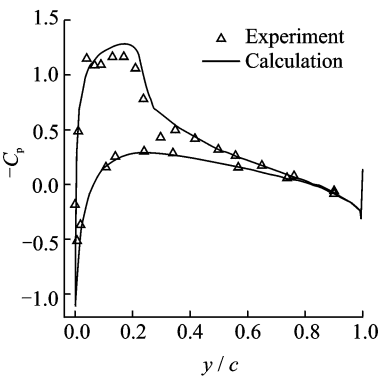

(c) 0.80R

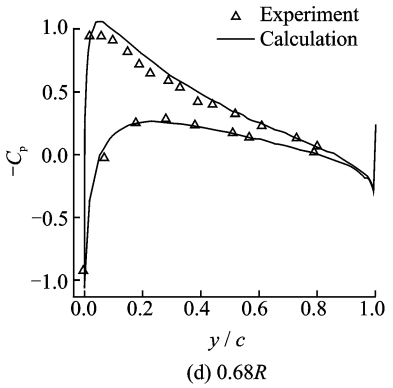

(d) 0.68R

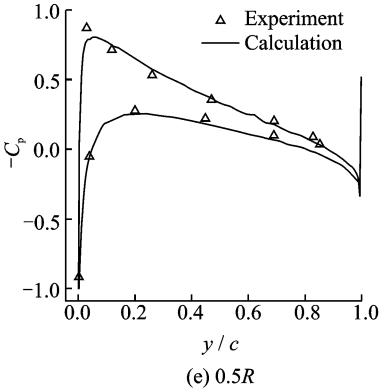

(e) 0.5R

Fig. 6 Distribution of surface pressure coefficient on different cross sections

sure coefficient C_p on different cross sections. As shown in Fig. 6, the computational results agree well with the experimental data, which indicates the validity of numerical methods.

3.2 Effects of tip slots on the rotor blade tip vortex

The computational model of the rotor with tip slots is shown in Fig. 1. For the grid of the rotor blade with tip slots, a very dense grid was generated in and around the slot before initial calculation as shown in Fig. 7. Due to the large range of tip vortex motion, it is unbearable to generate very dense grid in the whole computational domain. So the adaptive grid refinement technique was used to capture the blade tip vortex. The grid was adapted once when the rotor rotates a certain angle, and was adapted 28 times in total. The number of the grid cells increased from 7.37 million to 24.23 million. Fig. 8 is the contrast of the computational grid near the rotor blade tip before and after grid adaptation.

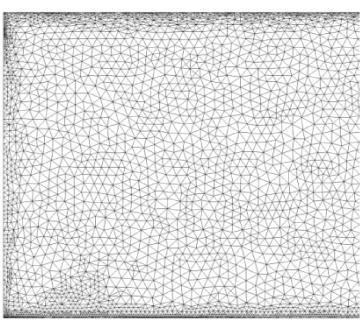

(a) Baseline tip

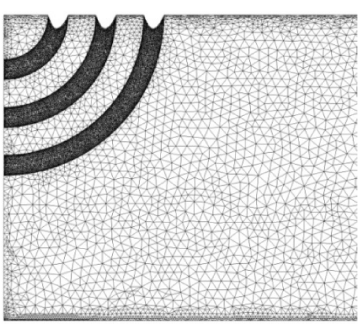

(b) Slotted tip

Fig. 7 Grid distribution of the rotor blade tip

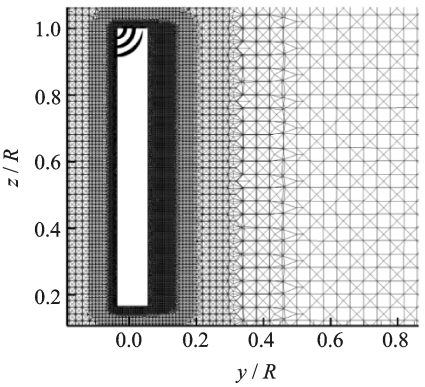

(a) Initial grid

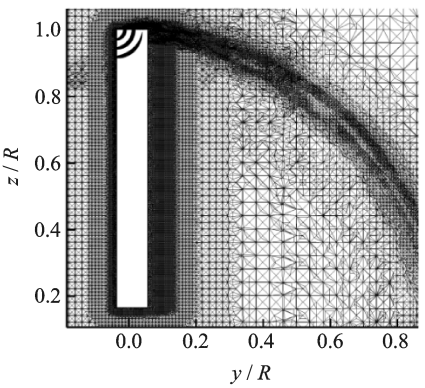

(b) Adaptive refined grid

Fig. 8 Contrast of computational grid near the rotor blade tip before and after grid adaptation

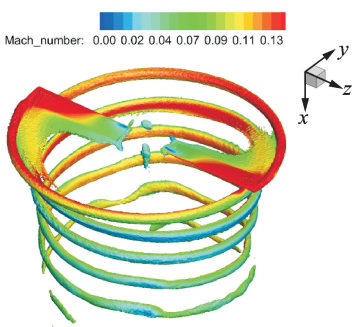

(a) Baseline tip

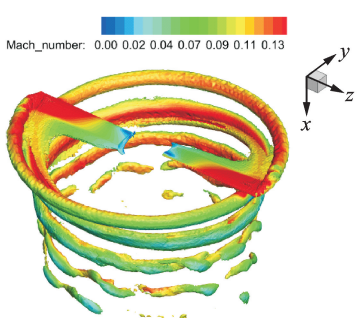

(b) Slotted tip

Fig. 9 Vorticity iso-surface of the rotor blade tip vortices with and without slots

Fig. 9 shows the vorticity iso-surface of the rotor blade tip with and without slots. It can be seen that the tip vortices develop continuously about 900° in the circumference direction for the rotor blade tip without slots, but only 540° for the rotor blade tip with slots[18]. Meanwhile, the

radius of the slotted rotor blade tip vortex is enlarged, which embodies the effect of tip slots on accelerating the dissipation of the blade tip vortex.

Fig. 10 shows vorticity distributions at the sectional plane across the core of the tip vortex, which are compared between the baseline tip and the slotted tip for several near-field wake ages. Compared with the baseline tip, the diameter of the vortex core of the slotted tip is larger and tip vortex strength is weaker. As the tip vortex migrates downstream away from the blade tip, the tip vortex of the blade tip with slots is quickly diffused, and the maximum vorticity is much small than that of the baseline blade tip, which demonstrates that tip slots can alleviate the rotor blade tip vortex effectively.

Fig. 11 shows the swirl and axial velocity distributions inside the core of the rotor blade tip vortex at 29° wake age, which are compared between the baseline tip and the slotted tip, where V_θ is the swirl velocity, V_{tip} is the blade tip velocity, V_{axial} is the axial velocity, and r represents the radial position. The swirl velocity of the vortex center is both 0, and there are opposite-sign peak values of swirl velocity on both sides of the vortex center. The distance between the vortex center and the peak values of the swirl velocity is defined as the radius of the vortex core[19]. As shown in Fig. 11, the swirl velocity increases gradually along the radial direction inside the vortex core and decreases outside the vortex core. For the slotted tip, the peak value of the swirl velocity decreases by 30%, and the axial velocity increases by 63% compared with that of the baseline tip. Since the greater the axial velocity of the vortex core is, the faster the blade tip vortex decays, the slotted blade tip vortex decays faster than the baseline blade tip vortex, which indicates that the rotor blade tip with slots can alleviate the tip vortex quantitatively.

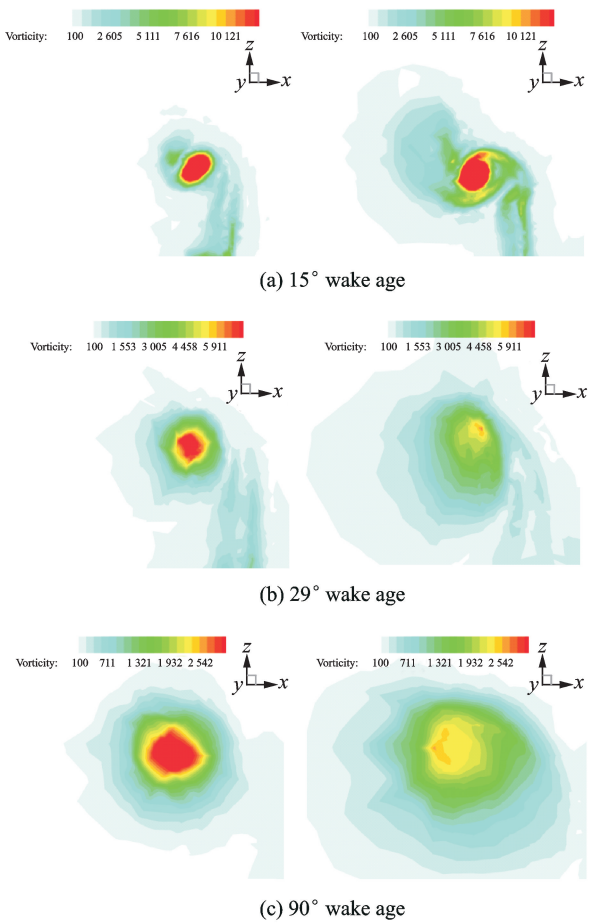

(a) 15° wake age

(b) 29° wake age

(c) 90° wake age

Fig. 10 Vorticity distributions at the sectional plane across the tip vortex core (the left figures show the vortex of the baseline tip, the right figures show the vortex of the slotted tip)

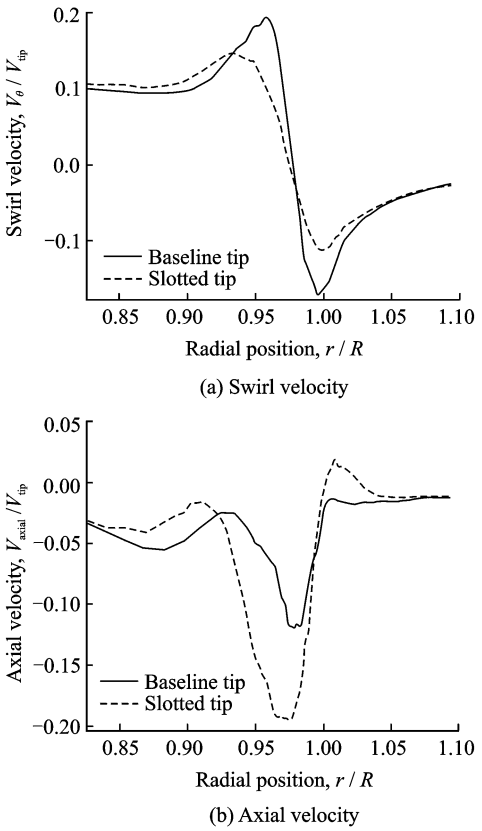

(a) Swirl velocity

(b) Axial velocity

Fig. 11 Swirl and axial velocity distributions inside the core of the tip vortex at 29°wake age

Since the pressure of the lower surface is larger than that of the upper surface, the air flowing bypass the blade tip from the lower surface to the upper surface generates the blade tip vortex. As shown in Fig. 12, the airflow ejected from the slot exit disturbs the airflow near the blade tip, enlarges the radius of the slotted tip vortex core and reduces the strength of the vortex, which reveals the mechanism that the blade tip with slots can alleviate the blade tip vortex.

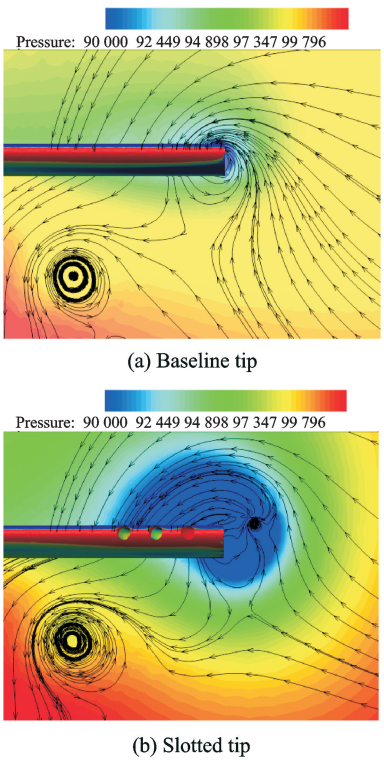

Fig. 12 Flow field of the cross section near the rotor blade tip ($y=0.37C$)

3.3 Effects of the blade tip with slots on the rotor aerodynamic characteristics

Fig. 13 shows the lift fluctuation T of the rotor with time. It can be seen that the lift of the rotor with baseline tip fluctuates periodically, while that of the rotor with slotted tip fluctuates more irregularly. The average lift of the rotor with or without tip slots is almost the same.

Fig. 14 shows the distribution of sectional lift coefficient C_l along the span of the rotor blade. When r/R is less than 0.82, the sectional airfoil lift coefficient of the rotor blade with tip slots is smaller than that of the rotor blade without tip slots. While r/R is greater than 0.82, the sectional airfoil lift coefficient of the rotor blade with tip slots is larger than that of the rotor blade without tip slots.

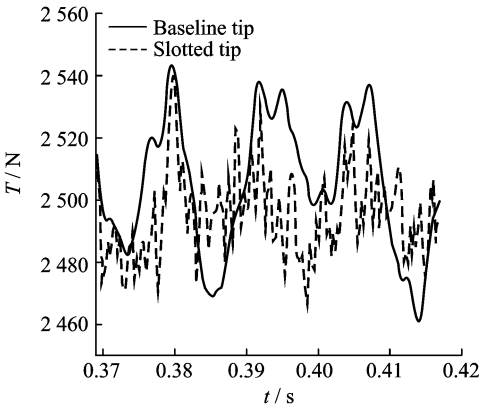

Fig. 13 Lift fluctuation of rotor with time

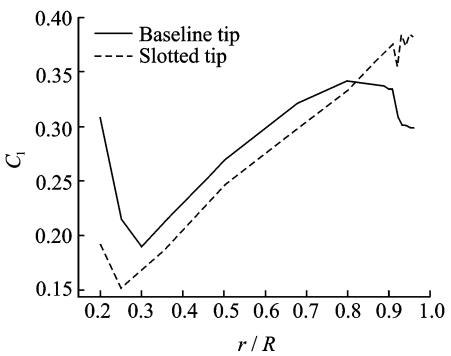

Fig. 14 Distribution of sectional lift coefficient along the span of the rotor blade

Fig. 15 shows surface pressure distributions of the rotor blade. It can be seen that the rotor blade tip slots reduce the intensity of the shock wave and form a larger low pressure area on the upper surface at the blade tip, while the tip slots reduce the range of the low pressure area on the lower surface. This is the reason why the sectional airfoil lift coefficient of the rotor with tip slots is larger at the blade tip.

Fig. 16 shows pressure distribution of the airfoil on different cross sections. At the section of $0.5R$, since it is far from the blade tip, there is little difference on the pressure distribution between the two types of rotor blade. At the section of $0.96R$, there is a strong shock wave standing on the upper surface of the airfoil for the baseline tip, while the shock wave is weakened for the

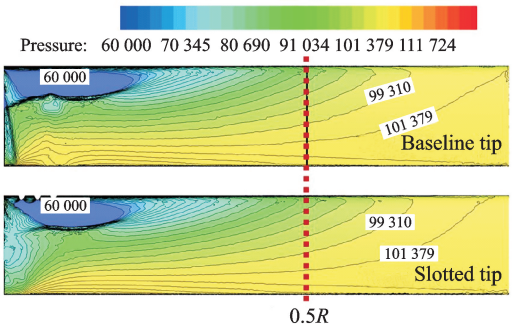

(a) The upper surface

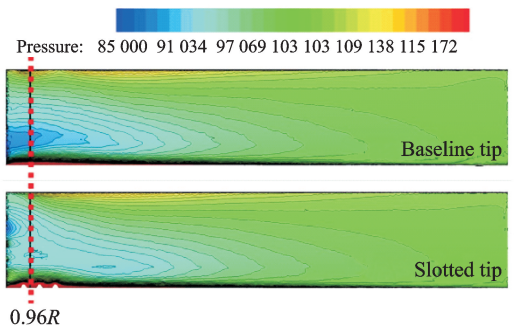

(b) The lower surface

Fig. 15 Surface pressure distributions of the rotor blade

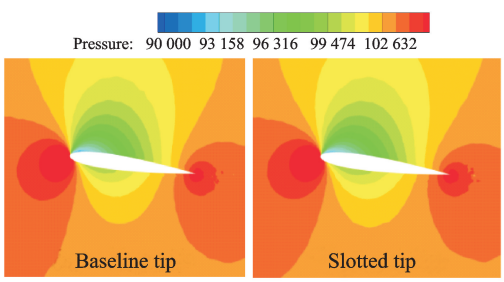

(a) 0.5*R*

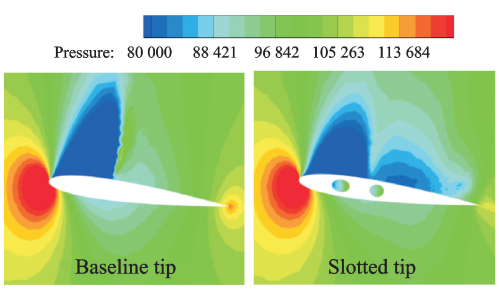

(b) 0.96*R*

Fig. 16 Pressure distribution of the airfoil on different cross sections

slotted tip, which results in a larger low pressure area on the upper surface for the slotted tip.

Fig. 17 shows the surface pressure coefficient C_p of the airfoil on different cross sections. At the section of 0.5*R*, there is little difference on the surface pressure coefficient between the two types of rotor blades. At the section of 0.96*R*, the strength of the shock wave is reduced and the lift of the airfoil is increased at the trailing edge, which results in the increase of the sectional airfoil lift coefficient at the rotor blade tip. This is consistent with the phenomenon reflected in Fig. 16.

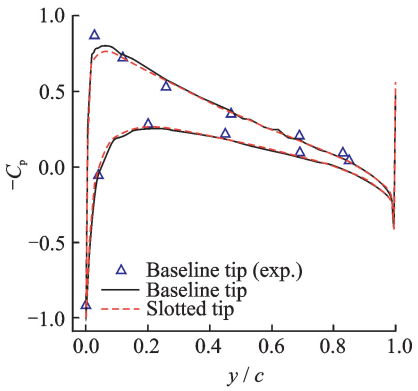

(a) 0.5*R*

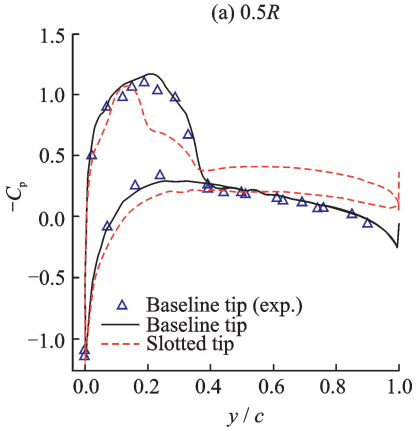

(b) 0.96*R*

Fig. 17 Surface pressure coefficient of the airfoil on different cross sections

4 Conclusions

Effects of tip slots on the aerodynamic characteristics of the helicopter rotor have been investigated numerically and the following conclusions can be drawn.

(1) The computational fluid dynamics (CFD) methods combined with IDDES model, the unstructured overset grids algorithm and the adaptive grid refinement technique are able to simulate the unsteady characteristics of the rotor blade tip vortex effectively. The computational result of surface pressure coefficient is in good

agreement with experimental data and the rotor blade tip vortices are captured well.

(2) The tip slot connecting the entrance at the leading edge to the exit at the side of the blade can enlarge the radius of the tip vortex, reduce the vorticity strength, and accelerate the dissipation of the tip vortex.

(3) Although the tip slot may lead to the decrease of sectional airfoil's lift coefficient at the root of the blade, it can increase sectional airfoil's lift coefficient at the tip of the blade, thus the lift of the rotor with tip slots is almost the same as that of the rotor without tip slots. Meanwhile, tip slots can also reduce the intensity of the shock wave, which is beneficial to reduce the wave drag of the rotor.

Acknowledgements

This work was supported by the Natural Science Foundation of Fujian Province of China (No. 2016J01029), the Aeronautical Science Foundation of China (No. 20155768007), and the National Natural Science Foundation of China (No. 11602209).

References:

[1] STERNFELD H. Advanced rotorcraft noise [J]. AIAA Journal, 2013, 24(2):107-109.

[2] SONG W P, HAN Z H, WANG L Q, et al. The effect of blade tip shape on rotor aeroacoustic noise by Euler Kirchhoff method [J]. Chinese Journal of Computational Physics, 2001, 18 (6):569-572. (in Chinese)

[3] SHI Y J, SU D C, XU G H. Research on influence of shape parameters on blade-vortex interaction noise of helicopter rotor [J]. Journal of Nanjing University of Aeroacoustics & Astronautics, 2015, 47(2):235-242. (in Chinese)

[4] BROCKLEHURST A, BARAKOS G N. A review of helicopter rotor blade tip shapes [J]. Progress in Aerospace Sciences, 2013, 56:35-74.

[5] YU Y H, TUNG C, BEREND V D W, et al. The HART-II test: Rotor wakes and aeroacoustics with higher-harmonic pitch control (HHC) inputs-the joint German/French/Dutch/US project [C]//Proceedings of the AHS 58th Annual Forum. [S. l.]: DLR, 2002.

[6] JACKLIN S A, BLAAS A, TEVES D, et al. Reduction of helicopter BVI noise, vibration and power consumption through individual blade control [C]// Proceedings of the AHS 51st Annual Forum. [S. l.]:NTRS, 1995:662-680.

[7] SIM B W. Suppressing in-plane, low frequency helicopter harmonic noise with active controls [C]//Proceedings of the AHS 64th Annual Forum. [S. l.]: [s. n.], 2008.

[8] HAN Y O, BAE H. Modification of the tip vortex by span wise slots [J]. KSAS Korean Journal, 1998, 27(5): 1-7.

[9] HAN Y O, CHUNG W J. Mean and turbulent characteristics of tip vortices generated by a slotted model blade [J]. Engineering Turbulence Modeling & Measurements, 2002,5: 637-646.

[10] HAN Y O, LEISHMAN J G. Investigation of helicopter rotor-blade-tip-vortex alleviation using a slotted tip [J]. AIAA Journal, 2004, 42(3):524-535.

[11] YOU J Y, KWON O J, HAN Y O. Viscous flow simulation of rotor blades with tip slots in hover [J]. Journal of the American Helicopter Society, 2009, 54:12006-1-12006-9.

[12] SHUR M L, SPALART P R, STRELETS M K, et al. A hybrid RANS-LES approach with delayed-DES and wall-modelled LES capabilities [J]. International Journal of Heat & Fluid Flow, 2008, 29(6): 1638-1649.

[13] SPALART P R. Detached-eddy simulation [J]. Annual Review of Fluid Mechanics, 2009, 41(1): 181-202.

[14] SPALART P R, JOU W H, STRELETS M, et al. Comments on the feasibility of LES for wings, and on a hybrid RANS/LES approach[C]//First AFOSR International Conference on DNS/LES. Louisiana, USA: Greyden Press, 1997:137-147.

[15] SPALART P R, DECK S, SHUR M L, et al. A new version of detached-eddy simulation, resistant to ambiguous grid densities [J]. Theoretical and Computational Fluid Dynamics, 2006, 20(3): 181-195.

[16] CHEN R Q, WANG X, YOU Y C. Numerical investigation of nacelle's effects on propeller slipstream based on IDDES model [J]. Acta Aeronautica et Astronautica Sinica, 2016, 37(6):1851-1860. (in Chinese)

[17] CARADONNA F X, TUNG C. Experimental and analytical studies of a model helicopter rotor in hover [J]. Vertica, 1981, 5(2):149-161.

[18] SUN W, GAO Z H, HUANG J T, et al. Aerodynamic characteristics of hovering rotor/wing [J]. Acta Aerodynamica Sinica, 2015, 33(2): 232-238. (in Chinese)

[19] XIAO Z Y, JIANG X, CHEN Z B. Numerical simulation of flow control on blade tip vortex of hovering rotor by slotted blowing [J]. Journal of Nanjing University of Aeroacoustics & Astronautics, 2016, 48(2): 165-172. (in Chinese)

Dr. **Chen Rongqian** is the associate professor in Xiamen University. He received his Ph. D. degree in Nanjing University of Aeronautics and Astronautics in 2012. His research focuses on computational fluid dynamics and aerodynamic design of aircraft.

Mr. **Wang Xu** is the engineer in AECC Hunan Aviation Powerplant Research Institute. He received master's degree in Xiamen University in 2017. His research focuses on computational fluid dynamics.

Mr. **Cheng Qiyou** is the senior engineer in Science and Technology on Rotorcraft Aeromechanics Laboratory, China Helicopter Research and Development Institute. His research focuses on rotorcraft aerodynamics.

Dr. **Zhu Chengxiang** is the assistant professor in Xiamen University. He received his Ph. D. degree in University of Stuttgart in 2014. His research focuses on computational fluid dynamics.

Dr. **You Yancheng** is the professor in Xiamen University. He received his Ph. D. degree in Nanjing University of Aeronautics and Astronautics in 2008. His research focuses on computational fluid dynamics and aerodynamic design of aircraft.

(Production Editor: Zhang Huangqun)